The Spatial and Temporal Variations of Turbulence in a Solar Flare

Northumbria University NEWCASTLE

Morgan Stores[1], Natasha, Jeffrey[1], Eduard Kontar[2]
morgan.stores@northumbria.ac.uk, natasha.jeffrey@northumbria.ac.uk, eduard.kontar@glasgow.ac.uk
[1] Department of Mathematics, Physics & Electrical Engineering, Northumbria University, Newcastle upon Tyne, UK, NE1 8ST
[2] School of Physics & Astronomy, University of Glasgow, Glasgow, G12 8QQ, UK

The detailed study of turbulence presented here suggest that turbulence has a more complex temporal and spatial structure than previously assumed, while the newly introduced turbulent kinetic energy maps help to identify important spatial inhomogeneities in the macroscopic plasma motions leading to turbulence.

Non-thermal Broadening of Spectral Lines

Turbulence is believed to be vital in accelerating particles during solar flares (Larosa & Moore 1993, Kontar et al. 2017). Non-thermal broadening (velocity) of spectral lines (Del Zanna & Mason 2018) in plasma is a key sign of the random plasma motions that can lead to turbulence. Here, non-thermal velocity is mapped across a flare in order to determine how it changes across different flare features (coronal loop tops, loop legs, close to ribbons).

- Spectral line profiles are obtained from the *Extreme-ultraviolet Imaging Spectrometer* (EIS) on the *Hinode* spacecraft and used alongside images from *Atmospheric Imaging Assembly* (AIA) aboard the *Solar Dynamic Observatory* (SDO) to identify key flare features.
- To find the line broadening, $\Delta\lambda$, Gaussian fits, were applied to spectral lines (Fig. 1): Fe $_{\text{XVI,}}$ Fe $_{\text{XXIII}}$ & Fe $_{\text{XXIV}}$ formed at temperatures 6.3 MK to 15.8 MK using,

$$I(\lambda) = I_B + I_0 \exp\left(-\frac{(\lambda - \lambda_0)^2}{2\Delta\lambda^2} \right)$$

- The line Full Width at Half Maximum (FWHM) is determined and the non-thermal velocity (v_{nth}) is calculated by rearranging,

$$\text{FWHM} = \sqrt{4\ln 2 \left(\frac{\lambda_0}{c}\right)^2 \left(\frac{2k_B T_i}{m} + v_{\text{nth}}^2\right) + \text{FWHM}_{\text{I}}^2}$$

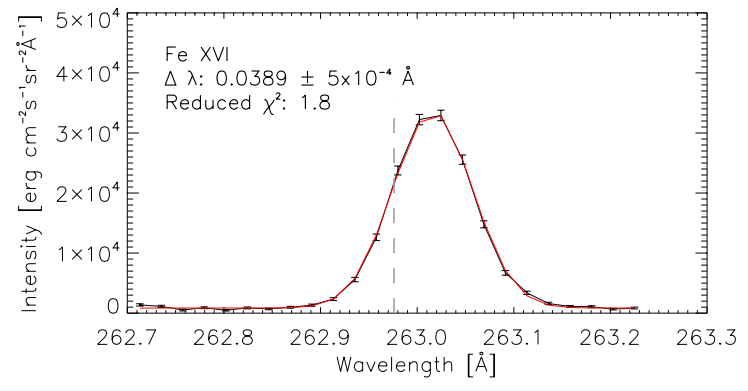

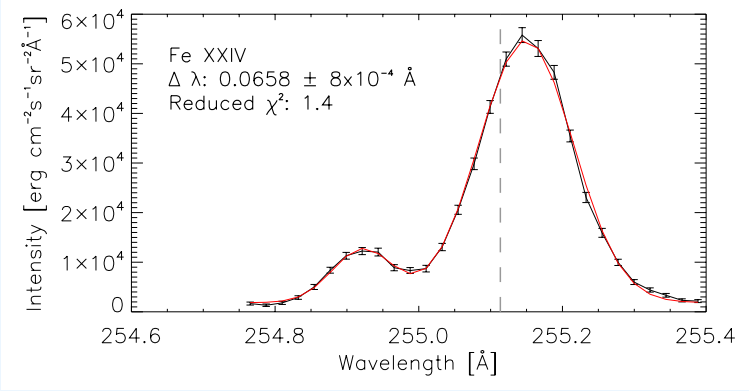

Figure 1 Example of the spectral line data (black) fitted with a Gaussian fit (red), and showing broadening Δλ and goodness of fit χ2.

Non-Thermal Velocity Maps

- The maps in Figure 2 show non-thermal velocity across the flare, from the coronal source to the ribbon features.
- The space-averaged non-thermal velocity across the flare (Fig. 3) is greatest in the hottest ions, Fe XXIII and Fe XXIV, and in general reduces with ion temperature (similar to previous observations (Antonucci et al 1995) and modelling (Gordovskyy, M. et al. 2016) results.)
- For the cooler ion, Fe XXIV, non-thermal velocity is almost constant as the flare progresses, slightly increasing.

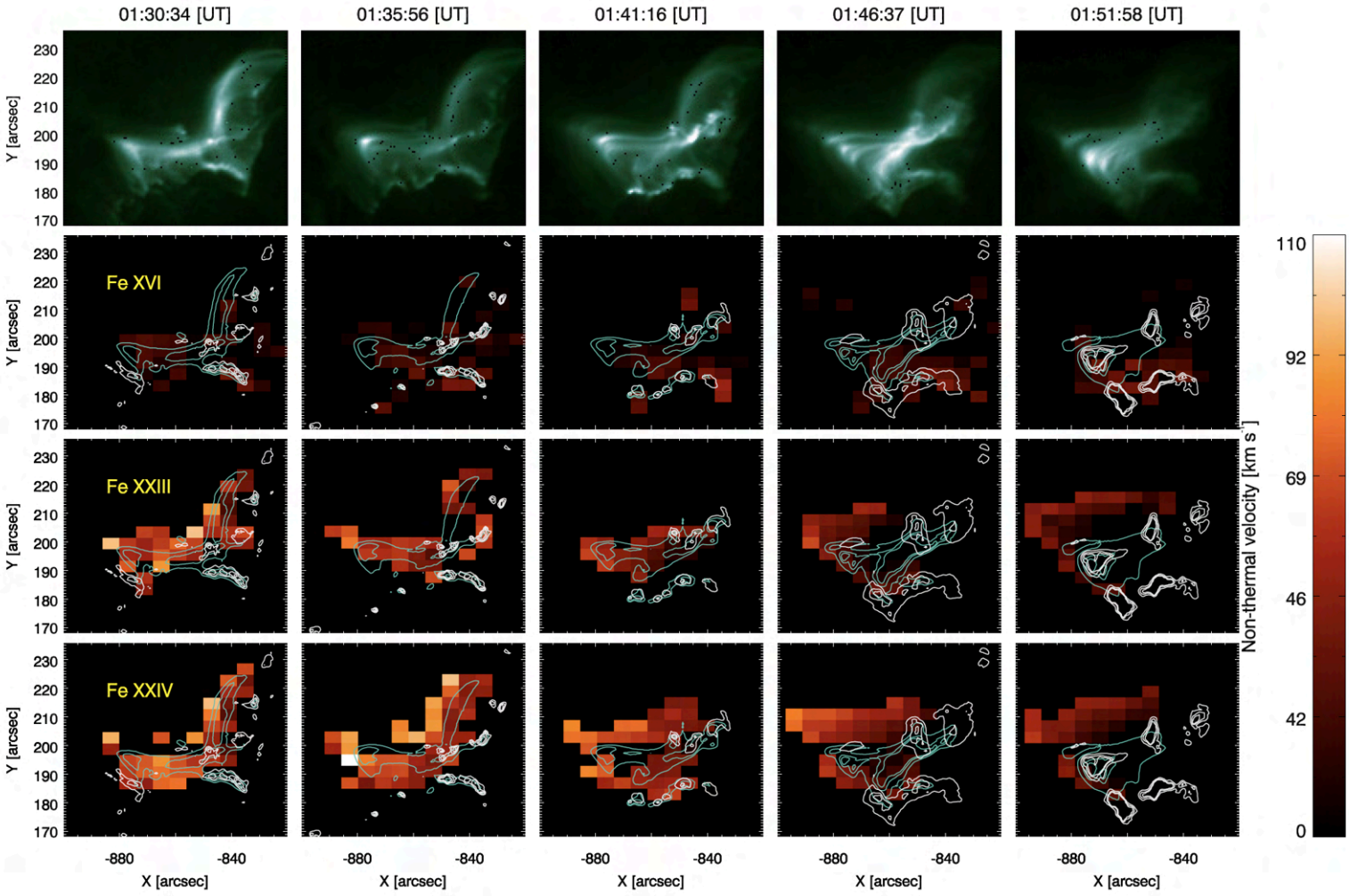

Figure 2 Maps of v_{nth} , and AIA 94 Å images (*top*), for each ion at times 01:30:34 to 01:51:58 UT. Rows 2-4, Fe XVI, Fe XXIII and Fe XXIV (top to bottom). The AIA 94 Å and 304 Å intensity levels overlaid onto the v_{nth} maps denote the flare cusp and hot loops (green) and ribbons (cyan).

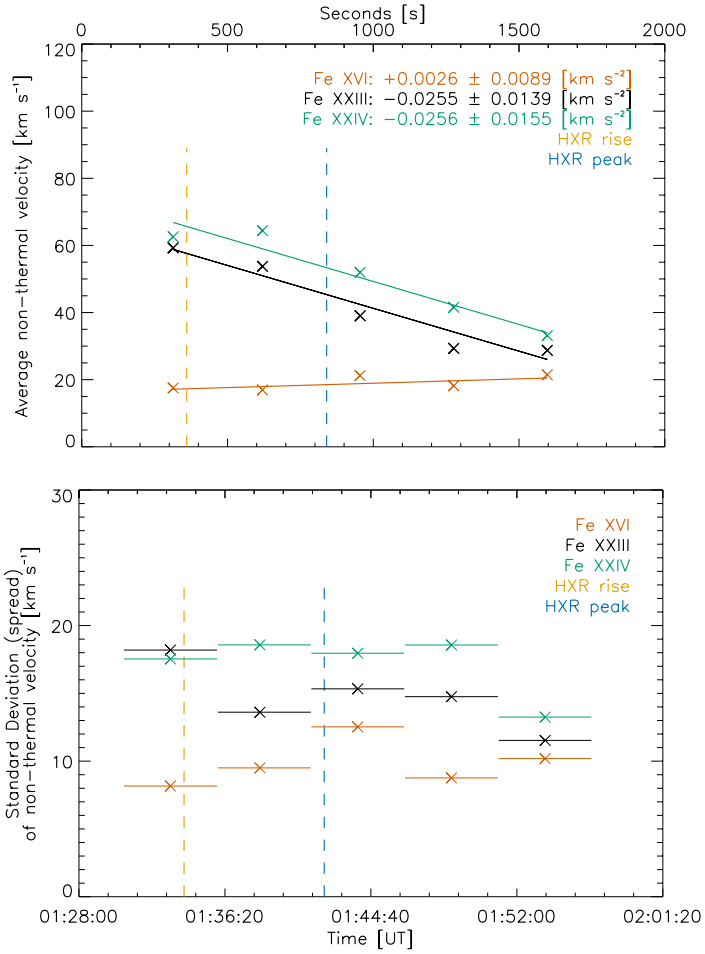

Figure 3 Spaced-averaged v_{nth} and standard deviation (spread) of v_{nth} for Fe XVI (orange), Fe XXIII (black) and Fe XXIV (green). Hard X-ray (HXR) emission peaks at ~01:34 UT and soft X-ray peak (SXR) is at 01:38 UT.

Analysing Non-Thermal Velocity Maps

Changes in time: Coronal Loop Tops

AIA data show multiple loops in the flare, comparing each loop top region in the hotter ions (Fig. 4 top), shows that at a given time the largest values of $v_{\rm nth}$ occur at the greater radial distance so that $v_{\rm nth}$ ('loop top 3': purple) > $v_{\rm nth}$ ('loop top 1': pink) > $v_{\rm nth}$ ('loop top 2': blue).

Changes in time: Southern Ribbon Feature

In the cooler ion Fe XVI, the $v_{\rm nth}$ of the extracted region (Fig. 4 middle), initially increases and peaks, coinciding with the rise and peak in HXRs, respectively. After the peak in HXR, $v_{\rm nth}$ of the extracted region begins to decrease. By the last time, at 01:51:58 UT, the value of $v_{\rm nth}$ is approximately the same value as the $\langle v_{\rm nth} \rangle$ for the entire flare.

Changes in space

Considering the line connecting the loop apex and along the loop leg (blue; Fig. 4 bottom):

- The $\langle v_{\rm nth} \rangle$ decreases at a similar rate for Fe xxiii ($dv_{\rm nth}/dx = -1.168 \pm 0.095$ km s^{-1} arcsec^{-1}) and Fe xxiv ($dv_{\rm nth}/dx = -1.08 \pm 0.081$ km s^{-1} arcsec^{-1}).
- At 01:51:58 UT, the non-thermal velocity for Fe xxiv is approximately ~20-25 km s^{-1} lower than at 01:46:67 UT but the values decrease along x at roughly the same rate of $dv_{\rm nth}/dx = -1.180 \pm 0.180$ km s^{-1} arcsec^{-1}.
- The decrease in $v_{\rm nth}$ is approximately linear at times corresponding to the peak in HXRs and after.

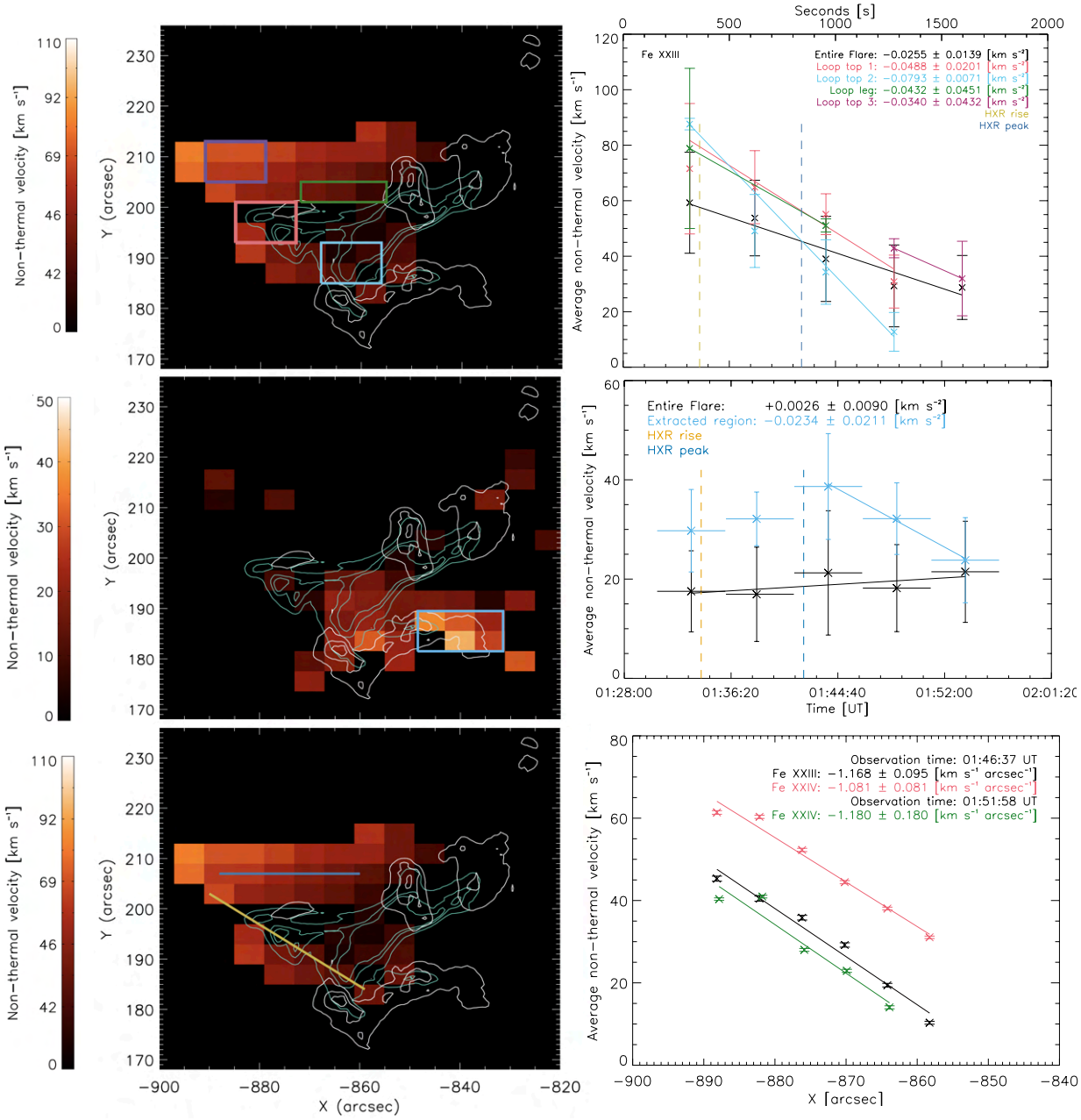

Figure 4 Analysis of non-thermal velocity maps. Changing $v_{\rm nth}$: (*Top*) with time for different coronal regions; (*middle*) with time close to a ribbon feature; (*bottom*) in space along a line connecting a loop apex to a loop leg.

Turbulent Kinetic Energy Maps

Creating spectral density diagnostics (Fig. 5 top), using the Fe XIV (264.7889 Å/ 274.2037Å) intensity ratio, allow the kinetic energy for the random motions in the non-thermal velocity maps to be calculated using,

$$\langle K \rangle = \frac{3}{2} \cdot 1.3 m_p \langle v_{\rm nth} \rangle^2 n_p V .$$

Kinetic energy density maps, show that:

- Cooler regions see high values of the kinetic energy density denoted by the Fe XVI emission. In particular, regions close to the flare ribbons, where the Fe XVI non-thermal velocity increased prior to peak in HXR emission, the larger number densities produce large values of kinetic energy density in the region.
- Large parts of the flaring corona show an almost identical reservoir of kinetic energy from turbulent motions; particles could extract this energy in the form of acceleration and heating in multiple parts of the flare.

Discussion and Conclusion

- Non-thermal broadening, indicating turbulence, was found to be present in all features across the flare, and in both hotter and cooler lines.
- Non-thermal broadening in hotter ions increased in the coronal source, and in space reduced towards the ribbon features in the chromosphere.
- Turbulence is distributed throughout the entire flare; often greatest in the coronal loop tops and decaying at different rates at various locations in the flare.
- Kinetic energy density maps suggest that similar levels of kinetic energy may be available in regions away from the loop apex.
- This study should be of interest to the modelling community and help to constrain the mechanism of turbulence in flares and its spatial and temporal distributions which are of great importance to the production and form of accelerated electrons in flares.

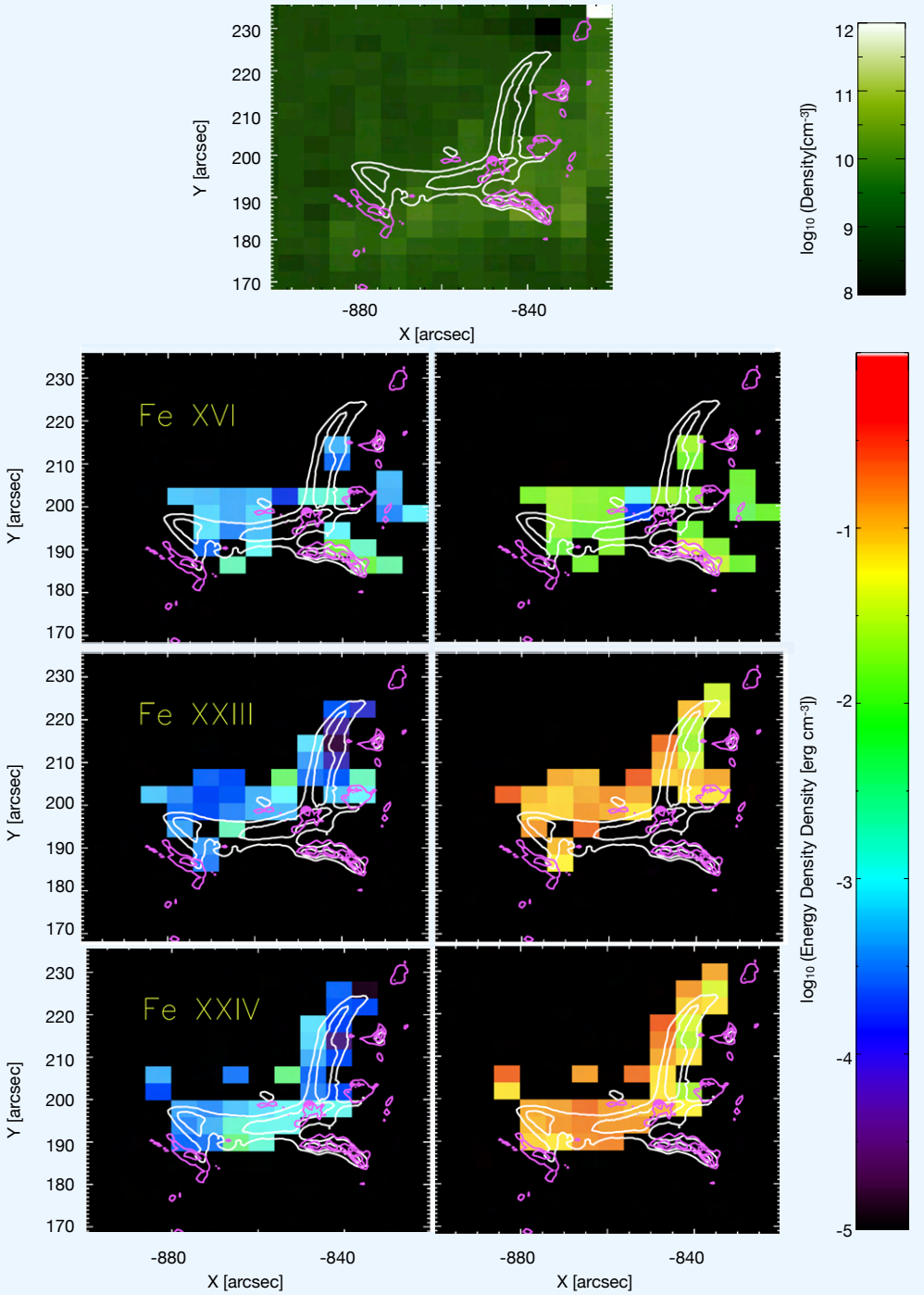

Figure 5 Density (log10) maps (*top*) using Fe XIV density diagnostics and kinetic energy density (log10) maps (*rows 2-4*) for for Fe XVI, Fe XXIII & Fe XXIV made with EIS density ratio (*left*) and average coronal density from X-ray observations in Kontar et al. (2017) (*right*).